MSURJ McGill Science Undergraduate Research Journal

Fabrication of optical fiber probes for scanning near-field optical microscopy

Si Yue Guo*, Jeffrey M. LeDue, Peter Grütter
Department of Physics, McGill University, 3600 University, Montreal, Canada, H3A 2T8

Abstract
Many areas of cell biology have remained unexplored due to the limitations of conventional optical microscopy for image structures smaller than the diffraction limit of light. Scanning near-field optical microscopy (SNOM) is an emerging technique which allows sub-diffraction limit optical resolution and hence access to nanoscale structures such as those in biological cells. Since the success of a scanning probe microscopy techniques depend on the tip, we present a method for the fabrication of SNOM aperture probes and antenna probes capable of high resolution imaging of delicate liquid based samples such as neurons. The procedure includes thinning and tapering optical fibers by chemical etching, followed by the deposition of a thin aluminium film, and micromaching using focused ion beam (FIB). Tip geometry, antenna resonances, excitation conditions, and field localizations have been examined. The probes have a resonant frequency of 18-28 kHz, a Q of 200-400 in air and up to 100 in water, and a spring constant of on the orders of 140 N/m. Successful optical and topographical imaging up to a resolution of 250 nm was achieved with the probes. Together with adjustments in equipment and instrumentation, the probe's optical and mechanical properties allow for a low imaging force and high tip sensitivity which are necessary conditions for the imaging of biological cells.

Introduction

The invention of the optical microscope at the end of the 16th century gave way to a whole new perspective of the world. Used in a diverse range studies, from biology to material sciences, conventional optical microscopy remains the most widespread imaging technique due to its simplicity, versatility, and non-invasive nature. The main disadvantage of the technique, however, remains its limited spatial resolution as predicted by Maxwell's equations. For standard microscopes setups, the equation yields a maximal optical resolution of ~ l /2 or around 250 nm for visible light (Paelser, 1996). With advances in science and technology, there has been a growing need to image at the nanoscale. In particular, there has been an interest in studying the features and mechanisms of biological cells which have thus far been unexplored.

In the last few decades, the development of high resolution microscopy techniques has sought to address this issue. Notably, three methods developed have been the most successful at surpassing the diffraction limit. In the 1970's, E. Ash and G. Nicholls were the first to surpass the limit by using the properties of evanescent waves for scanning in the near-field of a sample; the technique was called scanning near-field optical microscopy (SNOM), an idea first proposed by Edward Hutchinson Synge in the 1930's (Paelser, 1996). More recently, Stefan Hell developed stimulated emission depletion microscopy (STED), capable of attaining resolutions of tens of nanometers using the saturation of fluorescence inhibition by stimulated emission (Hell, 2003). Finally, Eric Betzig and his colleagues created a technique called photoactivated localization microscopy (PALM), where fluorescent molecules are activated one-at-a-time and an image is assembled from their positions (Betzig, 2006).

While all three microscopy techniques can be used to examine biological cells, SNOM is the only one that allows simultaneous mechanical measurements. A SNOM setup involves an atomic force microscope (AFM) with a modified cantilever probe that allows both optical and topographical imaging. For the latter, the probe scans the surface and deflects according to the changes in the interaction between the tip and the sample. Therefore, applied to imaging cells, it can optically resolve the locations of tagged proteins while determining how they influence the mechanical properties of the cell.

As with any scanning probe microscopy technique, the probe or the tip is the critical part of the instrument. Among the most successful SNOM probes are optical fibers tapered by chemical etching which employ sub-wavelength apertures (Paelser, 1996). These probes must be able to efficiently deliver light to the tip and properly image a sample at a high resolution. Additionally, recent research has shown that optical antennae, which are nanostructures resonant at optical frequencies, produce very well confined high electric fields. The combination of the sub-wavelength aperture with the optical antennae allows for a spatial resolution down to tens of nanometers (Taminiau, 2007).

Imaging biological cells presents several challenges and therefore any microscopy techniques needs to consider them. The soft and delicate cells necessitate a low imaging force so as not to destroy the samples. Also, since the sample is maintained in a liquid environment, special steps must be taken to ensure sufficient force sensitivity in the AFM. Hence, we are interested in characterizing and systematizing the fabrication process of SNOM probes that enhance the optical resolution and permit the imaging of biological samples.

SNOM Principle

Transmission mode scanning near-field optical microscopy (SNOM) relies on the efficiency of the probe to deliver light to the tip (Betzig, 1991), a schematic illustration of the SNOM principle is shown (Figure 1). In optical fibers, the probe is separated into three regions (Hecht, 2000). The first consists of a regular optical fiber waveguide where the difference in

Medium	Depth (•m)	Amp (mV)	Drive Amp (mV)	Drive Amp/Amp
air	0	107.927	81.35	0.8
water	230	101.318	100	1.0
water	280	98.694	220	2.2
water	330	94.727	350	3.7
water	380	95.337	700	7.3
water	430	94.055	900	9.6

Table 1: Drive efficiency of the SNOM probe as indicated by the ratio between the drive amplitude and the amplitude of the cantilever tunes

* Corresponding author. E-mail: siyue.guo@gmail.com

index of refraction between the core and the cladding allow for the total internal reflection of light. When the fiber tapers off and reaches the diameter of the glass core, a separate waveguide appears. Light reflects off the metal coating, which forms a conical metal-coated dielectric waveguide. As we approach the tip, only a single mode among the multiple modes remains. In this final region, light no longer propagates and the field is evanescent, escaping through the sub-wavelength aperture and exponentially decaying from the tip (Betzig, 1992). By placing the sample surface in the near-field of the SNOM probe ($< l/50$) (Betzig et al. , 1991), it is possible to surpass the diffraction limit. The spatial resolution depends on the size of the sub-wavelength aperture, which only illuminates the area directly below. Aperture probes are capable of imaging fluorescence, as well as metal structures and dielectrics.

A metal nanostructure resonant at optical frequencies acts as a quarter-wave antenna when placed next to the aperture of a SNOM probe (Taminiau, 2007). The local electric field at the edge of the aperture drives the antenna by providing an alternating current in the direction of the antenna (Taminiau, 2007). The electrons then move back and forth within the structure and create a standing wave of a quarter of the wavelength (node-antinode). In the far-field, the metallic protrusion acts like a dipole antenna but in the near-field, localizing the electric field distribution . Since the aluminium coating has a short penetration depth, optically, it behaves similarly like a perfect electrical conductor (Taminiau, 2007). In order for the electric field at the tip to have a maximum strength, the length of the antenna must be a multiple of $< \lambda/4$, with the thickness considered negligible compared the length. Since the antenna will be used only in the near-field, it is sufficient to note that the highly localized field formed at the antenna tip allows for the excitation of molecules in fluorescence imaging. The antenna hence becomes the main component in the imaging process (Figure 2). The resolution is not determined by the aperture size, but by the geometry and field localization of the antenna. In addition, the polarization of light which determines the field distribution at the edge of the aperture must be accounted for. From Figure 3, it is evident that the signal has maximal strength when the polarization of the light is aligned with the aperture and antenna (Figure 3b) and minimal strength when the polarization is completely misaligned (Figure 3c).

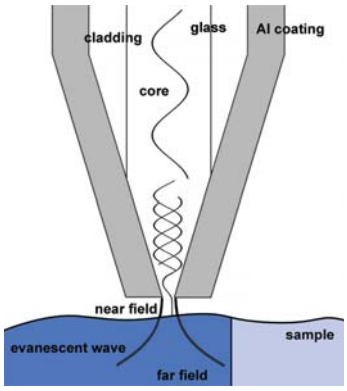

Figure 1: SNOM aperture probe. The transmission of light from the fiber to the surface of the sample and the three regions of the fiber tip.

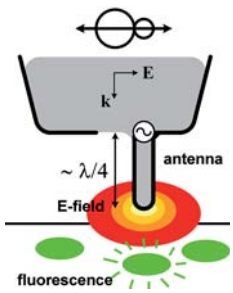

Figure 2: Fluorescence imaging with an antenna probe. The localized electric field at the tip of the antenna excites the molecules which fluoresce.

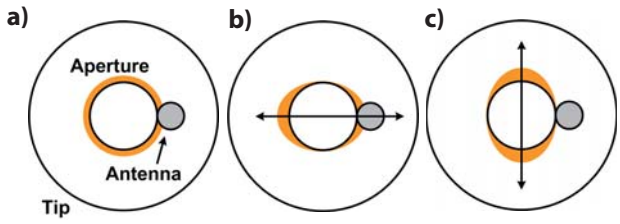

Figure 3: Polarization of light with respect to the aperture-antenna alignment (as indicated by the arrow), where a) no polarization, b) polarization aligned, c) polarization misaligned. The signal is greatest in b) where the polarization is aligned, and lowest in c) where it is completely misaligned, whereas in a) the distribution is even.

Experimental Setup

The setup of the transmission mode SNOM with a bent fiber probe is shown in Figure 4. It consists of a modified commercial atomic force microscope (Asylum Research) with an inverted optical microscope (Olympus), and a laser setup for optical imaging. An AFM uses a microcantilever to scan the surface of a sample. The piezo oscillates the fiber probe

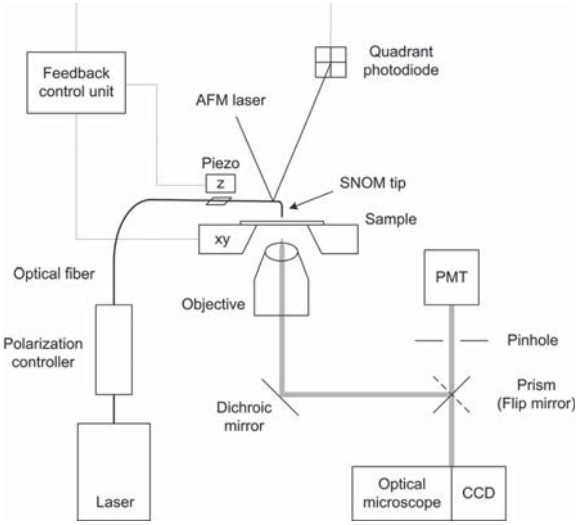

Figure 4 : Transmission mode SNOM setup schematic

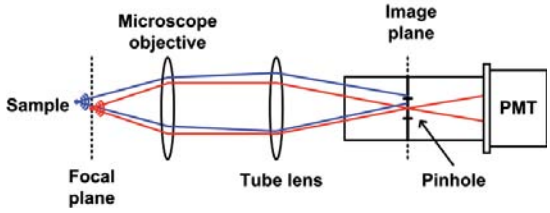

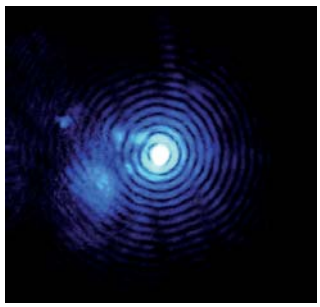

Figure 5 : a) Confocal pinhole setup with b) the diffraction pattern produced by the tip observed after the pinhole

mSURJ McGill Science Undergraduate Research Journal

in the z-direction (up-down) at a specified frequency, while the scanner moves the sample in the xy-directions. The cantilever deflects according to the various forces between the tip and the sample, and the deflection is measured by a laser reflecting off of the cantilever into a photodiode. There are several imaging modes that can be used in SNOM. In tapping mode AFM, the drive frequency is constant and changes in the oscillation amplitude are measured. Since it alternates between having the tip in contact with the surface for high resolution and lifted off to avoid dragging, this mode overcomes the difficulties encountered by other AFM scanning methods, including friction, adhesion, and electrostatic forces. Another relevant mode is the non-contact mode where changes in the resonant frequency of the cantilever as it interacts with a sample are used to maintain a small tip-sample separation (Morita et al, 2002). In both cases, measurements from the laser beam deflection sensor are used to plot the topography of the sample.

SNOM employs a modified cantilever probe. While the surface is scanned, the sample is locally illuminated by the fiber tip which is coupled to the laser (488 nm Argon-ion). The AFM distance is regulated by laser deflection for topographical imaging and for maintaining the sample in the near-field. Optical features are captured by a simple confocal microscope setup with a pinhole and a photomultiplier tube (PMT). The sample can also be observed through the eyepiece or captured by the charged-coupled device (CCD) camera.

As illustrated in the confocal pinhole setup (Figure 5a), the light from the sample is first collimated by the microscope objective and then focused into the pinhole by the tube lens. The confocal pinhole allows the photomultiplier tube (PMT) to capture a thin section of the sample at the focal plane, rejecting out-of-focus features as well as background noise. This facilitates the focalization of the image and ensuring that the sample is in the near-field of the tip. The tip is brought into the focal plane and centered into the pinhole by observing the image of the laser through the aperture. Figure 5b is a photograph taken at the position of the PMT showing the diffraction pattern produced by the tip.

Probe Fabrication

Chemical Etching

The fabrication of SNOM probes requires the tapering of optical fibers to form a tip. Three procedures were employed: tube etching, selective etching, and meniscus etching. The methods can also be employed individually or successively, in various combinations, to achieve the optimal taper angle and tip geometry (Taminiau, 2007; Mononobe, 1996).

First, in tube etching, the fiber (FS-SN-3224a/b, 125 µm), with its arcylate jacket left on, is dipped into 48-50% aqueous hydrofluoric acid (HF) solution. The acid diffuses through the jacket towards the end of the fiber, etching inward and upward producing smooth tapers with sharp tips. Due to the protection from the jacket, temperature fluctuations and vibrations have little influence on the fiber, making the process very practical. However, the geometry of the tip is not consistent and often non-circular.

The second etching technique relies on the selective etching of the core and cladding of highly germanium doped fibers (PSC and FDC). The tip forms at the end of the fiber, which must be cleaved prior to immersion in a buffered HF acid solution (48-50% HF and 40% NH4F). The geometry of the tip is determined by the NH4F:HF:H20 volume ratio and the cladding to core etch rate ratio (Mononobe, 1996), allowing for the production of a consistently circular tip (Figure 6).

The third technique, the meniscus etching procedure developed and patented by Turner, involves dipping the fiber

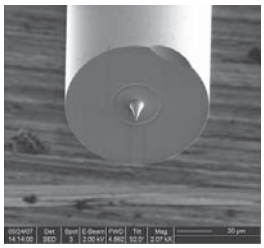

Figure 6 : Selectively etched tip (SEM)

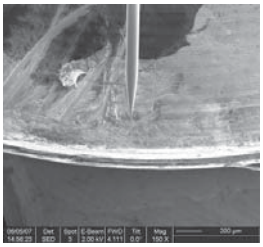

Figure 7 : Meniscus etched tip (SEM)

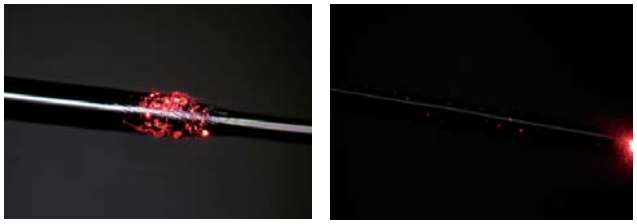

Figure 9 : Photographs of a tip coupled to a laser as viewed from under an optical microscope. We observe a)imperfections in the coating due to uneven etching at the meniscus of a thinned fiber and b) small pinholes along the taper of the fiber from dust particles in the solutions and a large pinhole at the tip.

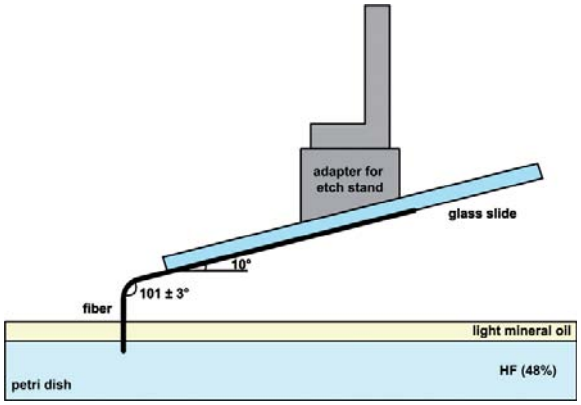

Figure 8 : Setup for etching bent fibers.

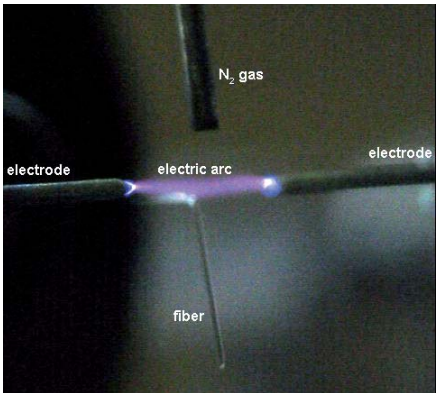

Figure 10 : Electric arc bending of optical fiber

into a solution of HF acid covered with an organic overlayer. Tapering occurs at the meniscus between the HF and the organic layer and it is usually ~ 300µm long (Figure 7). The acid etches completely through the fiber, eliminating the amount inside the solution; hence, the process is self-terminating (Turner, 1984). The angle of the taper is dependent on the nature of the overlayer and the stability of the solution. For instance, mechanical vibrations can lead to the production of rough fiber at the meniscus. Placing the etch stand on a cement block supported by rubber and wood blocks helps reduce these effects and produces smoother tips.

Since it is difficult to control the length of the fiber past the bend while bending it, an adapter for the etch stand is fabricated to taper already bent fibers. In Figure 8, we see the glass slide attached to the adapter at an angle of 10°. The fibers are placed perpendicularly on the slide and dipped into the solution. The length of the fiber that will remain past the bend is determined by the height of the slide and its distance to the bend. This allows us to achieve smaller and more accurate dimensions than obtained by bending etched fibers. This technique is not useful for selective etching, since the tip is formed at the cleaved end of the fiber, regardless of the amount submerged in the solution.

In addition to the formation of the taper, meniscus etching is also used to reduce the diameter of fibers. The entire length of fiber which will be used is submerged in the solution for a predetermined duration (based on the desired remaining diameter). Another etch, either meniscus or selective, is necessary to taper the tip.

Deposition of Aluminium Thin Film

Once the optical fiber is tapered, a metal coating is applied to create a conical metal coated waveguide, confining the light in the taper to the eventual aperture. A thin film of aluminium is deposited onto the SNOM probe in high vacuum (10-7 mbar) using a thermal evaporator 12. Aluminium has a short optical penetration depth, making it the ideal metal to coat the tip (Taminiau, 2007). For an even metal coat, the fibers are mounted onto a carousel attached to a motor rotating at 45° with respect to the direction of evaporation. The thickness of the aluminium coating varies between 150 nm and 500 nm, with a rate of deposition of 3-8 nm/s. While early techniques in SNOM aperture formation consisted of shadowing the tip during evaporation (Betzig, 1991), those techniques produce irregularly shaped apertures with large Al grains protruding past the tip. Instead, we allow the tips to be completely covered and create the aperture by FIB milling. It is important to check for pinholes by coupling the fiber to a laser and inspecting it under a microscope to ensure that the light will be properly transmitted to the tip. In Figure 9, various types of defects in the coating after meniscus etching are illustrated. The imperfections along the

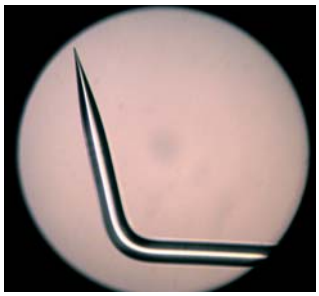

Figure 11 : Bent fiber, 105.6° (10x magnification)

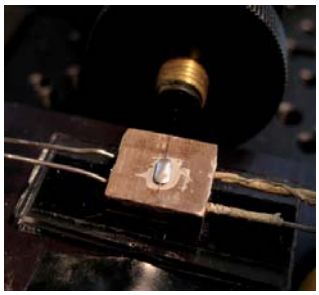

Figure 12 : Silver epoxy curing on heater plate

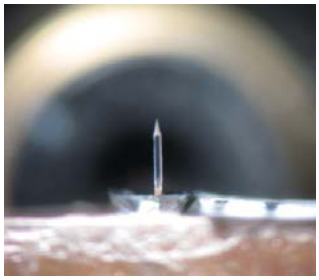

Figure 13 : Bent etched fiber perpendicular to chip

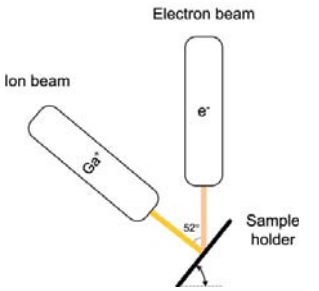

Figure 14 : Diagram of the dual beam SEM and FIB

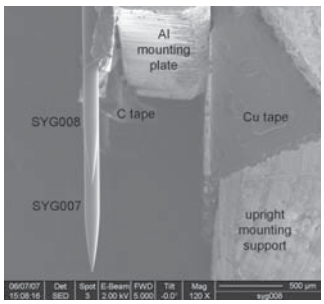

Figure 15 : FIB setup for upright fibers (SEM)

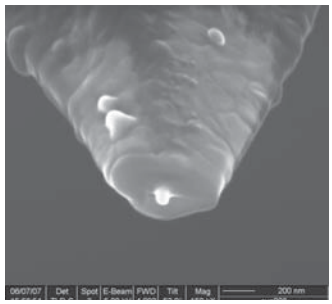

Figure 16 : Antenna on tube etched tip (SEM)

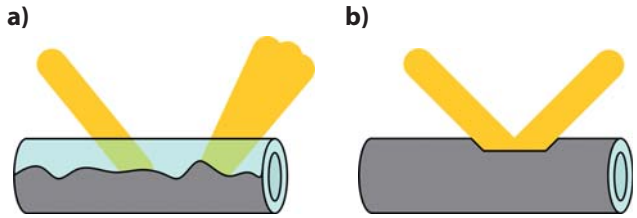

Figure 17 : Laser for AFM optical beam deflection a) passing through the fiber and bouncing off the bottom and b) bouncing off the reflective mirror surface

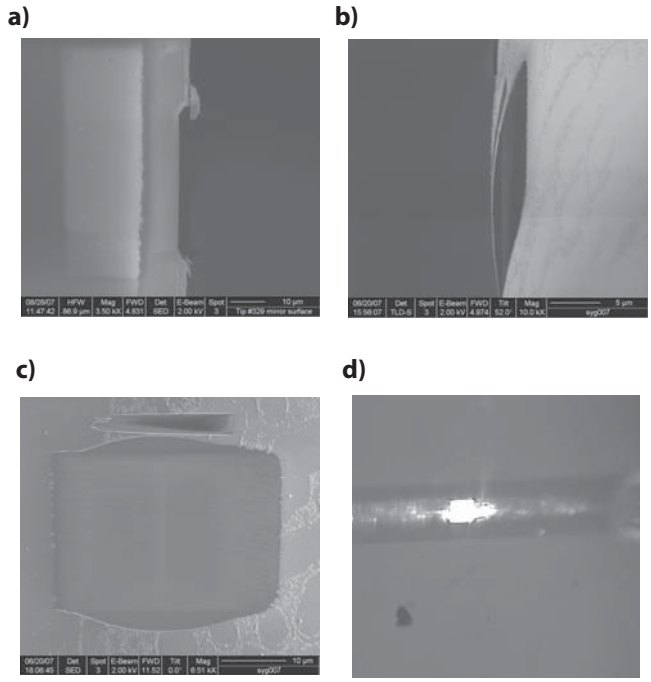

Figure 18 : Reflective surface a) lateral view b) side view c) top view d) top view with laser beam. a) – c) are taken with the SEM and d) is taken with a camera in the AFM.

mSURJ McGill Science Undergraduate Research Journal

length of the thinned fiber in Figure 9a)-b) are located far from the taper and the tip, and will therefore not disturb the transmission efficiency. However, the large pinhole at the tip of the fiber in Figure 9b is critical and renders the tip useless for SNOM. The small defects in the coating can be reduced by rigorously cleaning the fiber with filtered water. To eliminate large pinholes, all contact with the tip must be avoided.

Fiber Bending

For use in the AFM, the fibers are bent at an angle of 101° ± 3°, such that when mounted on the microscope, the tip lies perpendicularly to the plane of the samples. The two techniques most commonly used to bend fibers consist of CO2 laser heating and electric arc melting (Taylor, 1997). We employ a high frequency electric arc which heats and softens the fiber, which is then bent by the nitrogen (N2) gas flow and the force of gravity pulling down the tip (Figure 10). The exact angle of 101° is progressively obtained using successive trials with a measurement of the angle made after each trial. The bent fiber is photographed under an optical microscope and the angle is determined using image processing and analysis software. An intermediate step is shown in figure 11, where the desired angle is reached in less intermediate steps and with greater reproducibility by tilting the stage. This also results in a bend that is more even and consistently round because there is no need to reposition the fiber after successive bends.

Fiber Glueing

The bent fiber is glued onto a V-grooved cantilever chip (Figure 12) to be used in the AFM tip holder. We adjusted the position of the fiber so it to lies flat in the grove, extending 1mm past the edge and remains perpendicular to the plane of the chip. The right angle formed by the fiber and the cantilever chip is verified and corrected using photographs of the chip face on, such as in Figure 13. Silver epoxy is then delicately applied to the surface of the chip and cured until the glue hardens using a heater plate consisting of a current running through resistors.

Focused Ion Beam Milling

Micromachining the fiber tips using focused ion beam (FIB) (FIE DB235) milling allows for great versatility in the fabrication of structures. Figure 14 is a diagram of the system which includes a dual beam scanning electron microscope (SEM) and FIB separated by a 52° angle allowing for simultaneous SEM imaging and micromachining using gallium ions (Ga+). The sample holder tilts, allowing for cuts to be made with the ion beam.

Aperture and antenna formation

The formation of the aperture and the shaping of the tip require successive cuts made with the ion beam. The aperture is obtained by slicing off the tip of the fiber a couple hundreds of nanometers at a time until we observe a difference in contrast, usually indicative of the glass surface. The size of the aperture depends on the amount of the tip removed. For the fabrication of antenna probes, the tip is made by cutting the fiber on one side until we find the glass aperture. Then we remove the material on the other side to create a slice of metal on the edge of the aperture with a width corresponding to the intended diameter of our antenna. The probe is then rotated and mounted on the upright sample holder. The ridge is cut from both sides to carve the shape of the antenna (Taminiau et al., 2007). The setup created for this purpose is shown in Figure 15. The fibers are taped to a thin aluminium mounting plate with carbon tape, making it easy to manipulate them without modifying the orientation or disturbing the tip. This process is iterated until the desired geometry is obtained. An example of an antenna structure fabricated using the FIB is shown in Figure 16. Typical slice sizes are approximately 1 µm (L) x 0.3 µm (H) x 0.2 µm (W) with an ion-beam current of 10 pA for

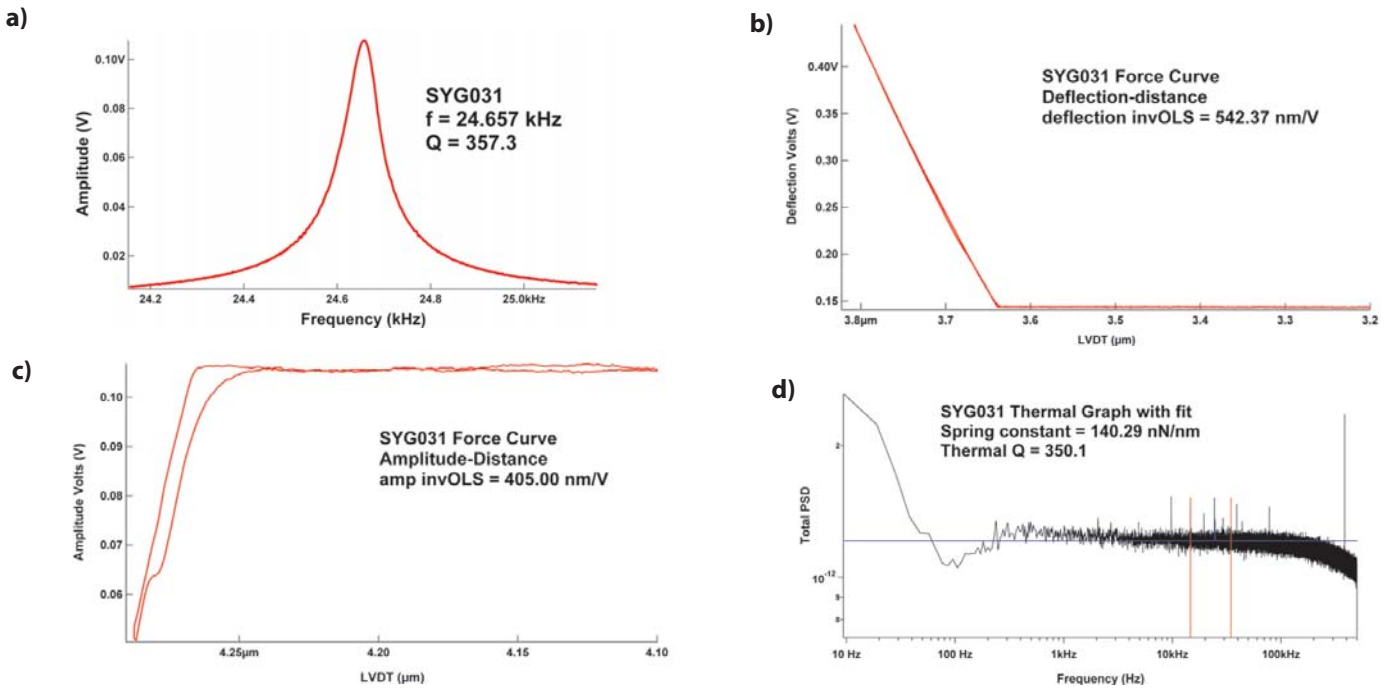

Figure 19: Graphs used in the measurement of the spring constant of tip (meniscus - selective etch) using the AFM: a)The cantilever tune, b) deflection-distance force curve, c) amplitude-distance force curve and d) thermal graph.

up to one minute.

Reflective surface

The initial method of reflecting the AFM laser beam for optical deflection consisted of bouncing the light off the bottom of a metal coated fiber (Figure 17a). However, any aberrations in the fiber and the coating can effect the shape of the beam returned to the detector, reducing the quality and the sensitivity of the beam. To solve the problem, a rectangle the size of the laser beam, 30µm x 60 µm, is cut from the top of the fiber using FIB milling. Once the fiber is coated with aluminium, the surface forms a flat mirror that returns the laser beam without changing its shape, as illustrated by Figure 17b.

Each cut is approximately 30 µm x 10 µm x 2 µm with a beam current of 5000 pA for an average of 10 minutes. Figure 18 is a collection of images of the reflective surface from various angles. As illustrated in Figure 18c, the surface is indeed flat and the laser can bounce off the mirror easily (Figure 18d).

Results and Discussion

Two sets of fiber probes were produced to test mechanical properties. The optical properties were studied using aperture probes provided by J. Ledue. The fibers in both sets were etched after being bent, using the tilted glass slide and etch stand adapter technique. In the first set, the full diameter of 125 µm of the fiber was preserved and the taper was formed by meniscus etch. We then explored the trade-off between size and our ability to fabricate them. For the second set, the fibers were first thinned to 60 µm by meniscus etch before tapering the tip. Due to the smaller dimensions, the thinner fibers were expected to have a better spring constant. There were no significant obstacles encountered due to size during the fabrication process.

Spring Constant

The spring constant of a tip can be measured using the thermal method which is included in the AFM operating software (Figure 19). This procedure calculates the constant using optical lever sensitivity and force-distance calibrations. Specifically, the cantilever tune gives the resonance frequency and the Q factor of the tip. The inverse optical lever sensitivity (invOLS) is obtained from the slopes of the deflection-distance and the amplitude-distance force curves. Finally, the spring constant is calculated from a thermal graph by comparing the peak to the background through Fourier analysis. The measured value of 140 N/nm, with an error of 10%, is comparable to theoretical spring constant of 137 N/m given the dimensions of the fiber. The spring constants for the limited number of fibers tested were of this order of magnitude.

Resonance Characteristics

The standard manufacturer's clip for the AFM tip holder consists of a rigid piece of stainless steel which cannot not be used for the SNOM probes. Compared to traditional AFM cantilevers, the SNOM tips require an opening for the tail of the fiber carrying light to the tip, which the original clip did not have, hence, several alternatives were tested. First, the probes were held in place by a thin sheet of copper bent into shape and anchored down with one screw. Although it was easily mounted and left room for the tail, this first clip did not provide sufficient pressure on the probe, so a second clip (Figure 20) was fabricated. The clip is made from 0.25 mm thick stainless steel foil, a tradeoff between the rigidity to clamp down the chip and the flexibility to allow the chip to oscillate in tapping mode AFM. The clip is held in place by two screws, giving the tip more stability and applying a more even pressure on the chip. In addition, the clamping force is easily adjustable for optimal drive efficiency in air and water by turning the screws.

To verify the effectiveness of the new clip, we examined the resonance curve of a tip held by each clip. Figure 21 shows the two cantilever tunes of a tip in air, obtained by the AFM which scans the range of frequency and records the amplitude of the oscillation as detected by the laser. We observe that the Q factor of the tip with the new clip is almost twice as great as that with the old clip. Since tapping mode AFM measures changes in amplitude of the oscillating cantilever caused by tip-sample forces, a higher Q (steeper resonance curve) means a larger change in amplitude for a given force. Thus, a higher Q improves the sensitivity of tapping mode AFM to force.

It is important to study the resonance characteristics of the SNOM probes in liquid, since it constitutes the medium in which many biological samples must be kept. We performed tests on a glass coverslip inside a sample holder containing water. The graph in Figure 22 shows the resonance curve of a tip as it slowly moves deeper from air into water. By continuously sweeping the drive frequency through the cantilever resonance peak, we are able to observe the exact moment when the tip touches the water, from the abrupt change in the appearance of the curve. We approximate the amount of fiber in contact with liquid at this point to be the length of the taper (~230 µm), where the meniscus forms and which was determined by meniscus etching. There is a first drop in Q factor and shift in resonance frequency, as shown by the red and orange curves. Figure 23 shows the Q factor as a function of the relative depth of the tip, where the reference point is when the tip first touches water. In addition, the drive effi-

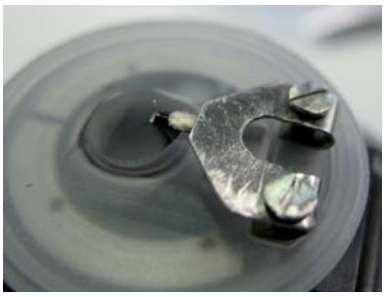

Figure 20 : New clip for the AFM tip holder

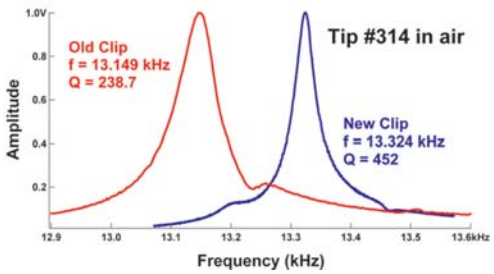

Figure 21 : Resonance curves of tip (courtesy of J. Ledue) with the new clip and the old clip.

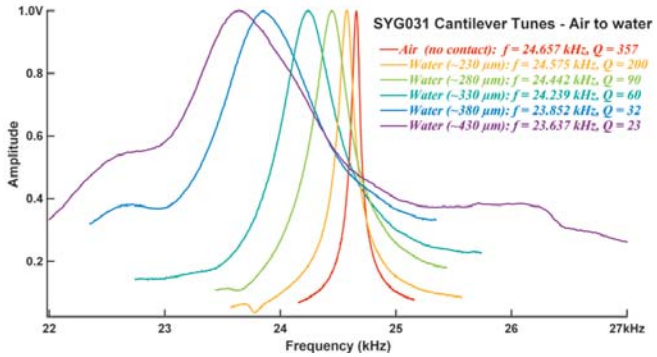

Figure 22 : Resonance curves of a tip (meniscus – selective etch) as it is lowered into the liquid from air. The curves have been normalized for the purpose of comparison. The original amplitude value is not relevant since it depends on the drive amplitude.

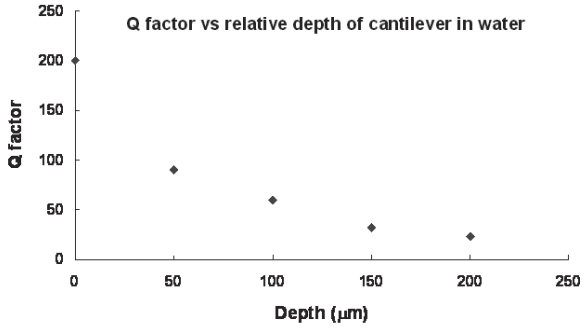

Figure 23 : Q factor vs. relative submerged depth of cantilever in water. The depth is measured from the point where the tip first touches water, so the first measurement in water is at 0μm with a Q of 200.

ciency, as indicated by the ratio between the amplitude and the drive amplitude is also worse as determined in Table 1. Afterward, the AFM head is lowered by 50 μm at a time until we no longer observe a change. The progressive decrease in Q factor, resonance frequency, and drive efficiency is consistent throughout the process. This is due to an increase in effective mass of the cantilever, as well as the drag force of the liquid which is affected by the depth of the tip in water. Nevertheless, the results show that it is possible to obtain good Q factors (60-90) in liquid compared to commercial cantilevers whose Q in water is around 10.

Imaging

The SNOM tips are capable of successfully imaging topographical features. Figure 24 is a three-dimensional image of the height trace of a sub-micron metal triangles calibration sample, imaged by a regular aperture-less probe. The image shows the most clearly defined features are displayed through the use of a slow scanning rate, 0.3Hz in this case.

The probes also allowed for fluorescence imaging (Figure 25). The microcontact printed stripes of the protein poly-l-lysine were imaged with fluorescent dyes FITC and Alexa 546, respectively, using an aperture probe (courtesy of J. Ledue and the Montreal Neurological Institute). In Figure 25a, the rectangular boxes of a darker shade represent areas bleached by the high intensity laser in previous scans. The round spots in both Figure 25a and b are most likely dust particles on the sample since they do not emit fluorescence. Finally, it has been verified from other scans that the diagonal features in Figure 25a and the dots in Figure 25b are indeed on the sample, which is an indication that our tips are able to pick up contrasts. The smallest features that appear in Figure 25b are measured to be on the orders of 250 nm, which is comparable to the diffraction limit of light.

Conclusion

We have determined and characterized the steps in the procedure for the fabrication of SNOM aperture probes and antenna probes and showed that the tapering of the optical fiber by chemical etching yields sharp, symmetric tips. The metal coating and subsequent FIB milling are effective methods for creating the aperture and antenna probes. As well, the techniques for mounting tips in the microscope, approaching the sample and imaging topography and fluorescence have been established.

Notably, we achieved high Q factors for the SNOM probes in liquid, as a result of modifications to the instrument such as insertion of a new clip. The ability to determine probe sensitivity by controlling the depth of the tip in liquid leads to the potential for very high probe sensitivity compared to that of commercial cantilevers in liquid. This makes the probes amenable to non-contact AFM imaging (Morita, Wiesendanger & Meyer, 2002), a technique which has the potential to provide lower forces than tapping mode AFM.

Finally, combined with the preliminary results regarding the aperture size and antenna shape, the SNOM probes should allow for unique combined optical and topographical imaging of biological samples, paving the way for a greater understanding of physical and biological mechanisms within cells.

Acknowledgments

I would like to thank Jeffrey LeDue and Professor Peter Grütter and as well as many other faculty and staff members in the Physics Department at McGill University for their collaboration, guidance, and assistance with the project. I would also like to acknowledge the support of Ms. Marie-Hélène Bernier and the central facilities of the École Polytechnique and the Université de Montréal funded by CFI, NSERC and NanoQuebec for SEM and FIB training and access to microfabrication laboratory. As well, the Montreal Neurological Institute has played a vital role by providing us with biologi-

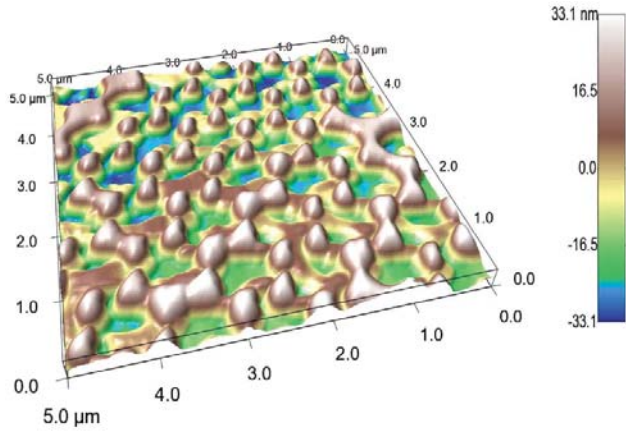

Figure 24 : Height trace of metal triangles with tip (meniscus etch).

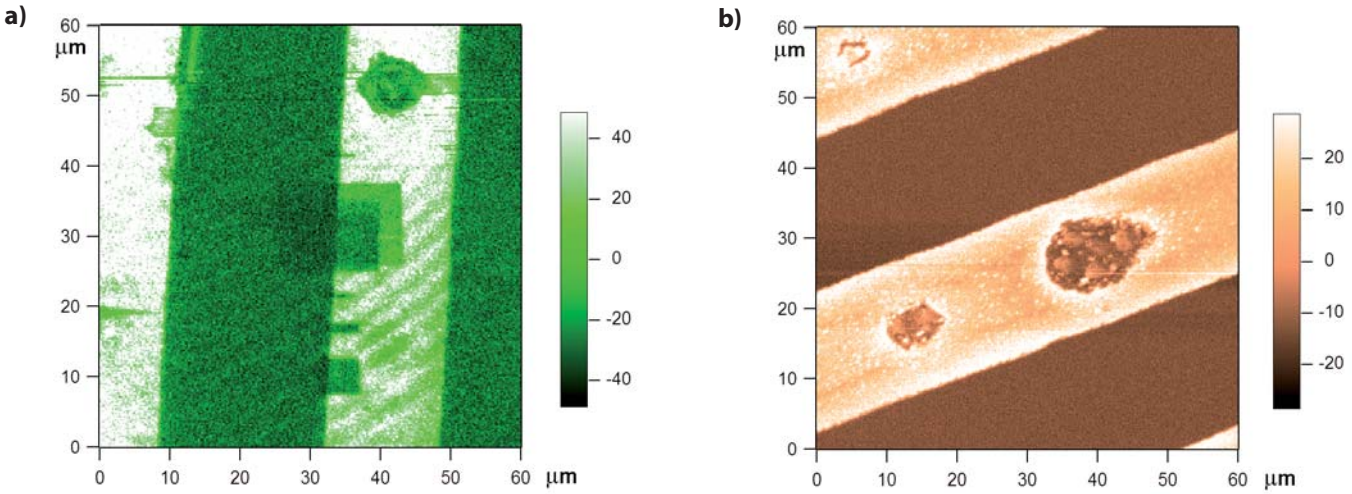

Figure 25 : The protein poly-l-lysine (20µm stripes) with fluorescent dyes a) FITC and b) Alexa 546 (AFM images courtesy of J. Ledue).

cal samples to image. Finally, I would like to thank my family and friends who have constantly supported my interests in science and my passion for research.

References

1. Betzig, E. et al. "Near-Field Scanning Optical Microscopy (NSOM): Development and Biophysical Applications", Biophysical Journal, vol. 49, 1986, p.269-179.
2. Betzig, E. et al. "Breaking the Diffraction Barrier: Optical Microscopy on a Nanometric Scale", Science, vol. 251, March 1991, p.1468-1470.
3. Betzig, E. & J.K. Trautman. "Near-Field Optics: Microscopy, Spectroscopy, and Surface Modification Beyond the Diffraction Limit", Science, vol. 257, July 1992, p.189-195.
4. Betzig, E. et al., "Imaging Intracellular Fluorescent Proteins at Nanometer Resolution", Science, vol. 313, September 2006, p.1642-1645.
5. Hecht, B. et al. "Scanning near-field optical microscopy with aperture probes: Fundamentals and applications", Journal of Chemical Physics, vol. 112, no. 18, May 2000, p.7761-7774.
6. Hell, S.W., "Toward fluorescence nanoscopy", Nature Biotechnology, vol. 21, no. 11, November 2003, p. 1347-1355.
7. LeBlanc, P.R. Dual-Wavelength Scanning Near-Field Optical Microscopy. Ph. D. thesis, McGill University, Canada, 2002.
8. Mononobe, S. & M. OHSTU. "Fabrication of a Pencil-Shaped Fiber Probe for Near-Field Optics by Selective Chemical Etching", Journal of Lightwave Technology, vol. 14, no. 10, October 1996, p.2231-2235.
9. Morita, S., R. Wiesendanger & E. Meyer. Noncontact Atomic Force Microscopy, Springer, 1st ed., 2002.
10. Paesler, M.A. & P.J. MOYER. Near-Field Optics: Theory, Instrumentation, and Applications, Wiley-Interscience, 1st ed., 1996.
11. Taminiau, T.H. et al. "λ/4 Resonance of an Optical Monopole Antenna Probed by Single Molecule Fluorescence", Nano Letters, vol. 7, no. 3, 2007, p.28-33.
12. Taminiau, T.H. et al. "Near-field driving of a optical monopole antenna", Journal of Optics A: Pure and Applied Optics, vol. 9, 2007, p. S315-S321.
13. Taylor, R.S. "Bent Fiber Near-Field Optical Microscopy Probes for Use With Commercial Atomic-Force Microscopes", Proc. SPIE, vol. 3009, 1997, p.119-129.
14. Turner, D.R. "Etch Procedure for Optical Fibers", U.S. Patent 4469554, 1984.